CORE
Metadata, citation and similar papers at core.ac.uk
Provided by Open Access LMU

PHYSICAL REVIEW A VOLUME 46, NUMBER 3 1 AUGUST 1992

Electron capture and loss to continuum from 200-keV/u H^0 and He^0 projectiles colliding with He and Ar targets

H. Trabold, G. M. Sigaud,* D. H. Jakubassa-Amundsen,† M. Kuzel, O. Heil,‡ and K. O. Groeneveld
Institut für Kernphysik der J. W. Goethe-Universität, D-6000 Frankfurt/Main, Germany
(Received 22 November 1991)

Electrons ejected in collisions with neutral hydrogen and helium projectiles (200 keV/u) into the forward direction are measured in coincidence with the charge-state-analyzed outgoing projectile (H^0, H^+; He^0, He^+, He^{2+}). All electron spectra, including those recorded in coincidence with H^0 and He^0 atoms, where the long-range Coulomb field is screened, show a cusplike structure. The data are compared with available theories for electron capture to the continuum.

PACS number(s): 34.10.+x, 34.50.Fa, 34.70.+e

I. INTRODUCTION

Since its observation by Crooks and Rudd [1] two decades ago, the cusp-shaped peak which appears in the 0° electron spectra at an energy $mv^2/2$, where v is the collision velocity and m is the electron mass, has provided interesting and new insights in both the structure and dynamics of atomic collisions [2]. In particular, it gives detailed information on the ionization processes of both the target and the projectile [3,4]. Until now, experimental and theoretical investigations on the capture of a target electron (ECC) or the ejection of a projectile electron (ELC) into low-lying continuum states of the projectile have mostly been restricted to cases where the projectile was bare or partially stripped [2,5]. In an ion-atom collision, the appearance of the cusp-shaped peak is currently explained in terms of the properties of the final electronic projectile continuum eigenstate, which for Coulombic fields has a diverging normalization constant at threshold. This induces a divergence of the doubly differential cross section (DDCS) and hence leads to a cusp in the measured forward electron spectra [6].

However, Sarkadi *et al.* [7] reported for the first time the observation of a cusp-shaped peak in the spectra of electrons captured by neutral projectiles. By measuring the emitted electrons in coincidence with the outgoing charge state of the ejectiles (i.e., the projectiles which have been involved in a collision and therefore have been ejected out of this process) for collisions of 75 keV/u He^0 with He and Ar targets, they were able to distinguish between the ELC and the ECC processes. For outgoing He^0, they found a forward peak which was even narrower than the one recorded in coincidence with He^+ or He^{2+} ejectiles. More recently, a similar behavior was found for a H^0 projectile colliding with Ar [8]. Cusp-shaped peaks associated with neutral ejectiles have also been observed in ion-solid collisions [9].

In order to understand such a remarkable phenomenon, several theoretical models have been developed. Assuming that the neutral projectile is in the ground state, electron capture to continuum has been calculated within the peaked-impulse approximation (IA) [10], using the low-energy scattering solution of a Schrödinger-type equation with a fully screened potential for the electronic projectile continuum eigenstate [11]. Although this model confirms the existence of a 0° forward peak for neutral ejectiles, the predicted peak width is considerably larger than the one found in experiment.

A different idea has been put forth by Barrachina [12] when trying to explain the He^0 results. It is based on the assumption that the neutral projectile is either in an excited metastable initial state or is excited during the collision prior to electron capture. In that case, the target electron may temporarily be captured into a low-lying virtual state of the negative projectile ion. Such a resonant behavior modifies the electronic projectile continuum eigenstate and in fact leads to a forward peak which may be very narrow, depending on the resonance parameters. This model, also applying the peaked IA, provides a peak shape which is very close to the data of Sarkadi *et al.* [7]. However, the probability for exciting the projectile in the same collision via the electron-electron coupling has been found to be at most 1% and hence the model relies on the presence of a considerable fraction of metastable states in the incoming beam.

A third possibility, somehow related to the Barrachina prescription, has been suggested by Szótér [13]. For the case of a He^0 projectile, a series of intermediate nonmetastable autodetaching states of the negative ion (He^0 plus active target electron) may be populated during the collision. These intermediate states would then act as sources for the cusp formation after the collision. However, quantitative estimates are not available for this picture.

Clearly, additional experimental data with well-defined initial projectile configurations are required to support or disprove the existence of a narrow cusp for neutral projectiles, and to discriminate between the various theoretical approaches. Therefore we have performed a systematic study of the electron-capture and -loss processes by measuring the spectra of electrons emitted in the forward direction ($\Theta = 0°$) in collisions of 200 keV/u H^0 and He^0 projectiles with He and Ar in coincidence with the emergent charge states of the projectiles. The He^0 pro-

 ©1992 The American Physical Society

jectiles were used not only to cross check and extend the results of Sarkadi *et al.* [7], but also to provide absolute values for the cross sections. However, the He^0 beam usually contains an appreciable fraction of metastable states. In order to have a well-defined initial configuration, ECC and ELC were also measured for a H^0 beam, which has the advantage that practically all projectiles can be prepared in their ground state. Also, when changing the projectile from H^0 to He^0, i.e., changing the projectile charge and adding one electron, differences in the electron-capture process attributed to the loosely bound projectile electrons can be identified.

In Sec. II the experimental setup and the data taking and reduction procedures are described. The theoretical approaches are discussed in Sec. III, and our experimental results in comparison with theory are presented in Sec. IV. Finally, the conclusion is drawn in Sec. V.

II. EXPERIMENT

The experiments were performed at the 2.5-MV Van de Graaff accelerator of the Institut für Kernphysik of the J. W. Goethe-Universität, Frankfurt/Main, which provided beams of H_2^+ and He^+ with energies of 200 keV/u. Figure 1 presents a schematic view of the beam line.

The neutral beams were obtained following two different procedures. For the He^0 projectiles, the original charged beam traversed a gas cell (in Fig. 1, gas cell no. 2) for electron capture, after being charge and momentum analyzed by a switching magnet. The neutral fraction was then electrostatically separated and quenched, in order to reduce metastable states, before entering the collision chamber. The fraction of excited metastable states of He^0 that still remains in the neutral beam after quenching is estimated to range from 25% to 35% [14]. The H^0 beam was produced in two steps: First, the original molecular ion H_2^+ was dissociated, mostly into H^0 and H^+, by traversing the gas cell no. 1, located before the switching magnet, which, thus, acted also as a charge-state analyzer; then, the H^+ beam so produced passed through gas cell no. 2, following the same procedure described above. We have used this method, because this was the only way to obtain a H^0 beam of 200 keV from our accelerator, which has a minimum operating voltage of 250 kV. The electrostatic separation and quenching of the neutral beams were achieved by means of two sets of parallel-plate deflectors, approximately 1.5 m apart, with voltages of 8.0 and ± 1.0 kV, respectively. These fields are sufficiently high to guarantee that, in the H^0 case, only ground-state atoms were present in the incoming beam [15]. The pressures in both gas cells were of the order of 10^{-5} mbar, while the pressure in the beam line was kept well below 10^{-6} mbar.

The neutral-beam path was predefined by two pairs of apertures. The first one, located between the two sets of deflection plates, consisted of a 0.8-mm-diameter collimator and a 1.0-mm antiscattering aperture, 10 mm apart. The second set, positioned 1.3 m downstream from the first and 95 mm ahead of the focusing point of the electron spectrometer, has a 0.6-mm-diameter collimating aperture with a 1.2-mm antiscattering one. This second pair is mounted on either side of the outer part of a double cylindrical support, 100 mm long, which is placed at the entrance of the collision chamber. A voltage of +400 V was applied to the inner cylinder with respect to the outer one, in order to eliminate beam-slit scattering halos produced along the beam path. The angular divergence after this collimation arrangement was $\Delta\Theta_p < 0.1°$. Further collimation, achieved by micrometrically movable slits, reduced the neutral-particle intensities to less than 100 counts per second, with a corresponding beam size of approximately 1 mm^2 in area.

We have used as targets He and Ar jets produced by a 1.0-mm-diameter needle output, mounted on a 250-mm-long tube with 2.5-mm internal diameter, which guaranteed a molecular-flow regime for the pressures used. The gas flow was automatically controlled by a high-sensitivity pressure gauge connected to a valve located upstream of the needle, the end of which was removed 0.5 mm out of the beam cross section.

The electron spectra produced in collisions between the gas-jet target and the incoming beams were measured by a cylindrical-mirror electron spectrometer, which is shown in Fig. 2, and is similar to the one described by

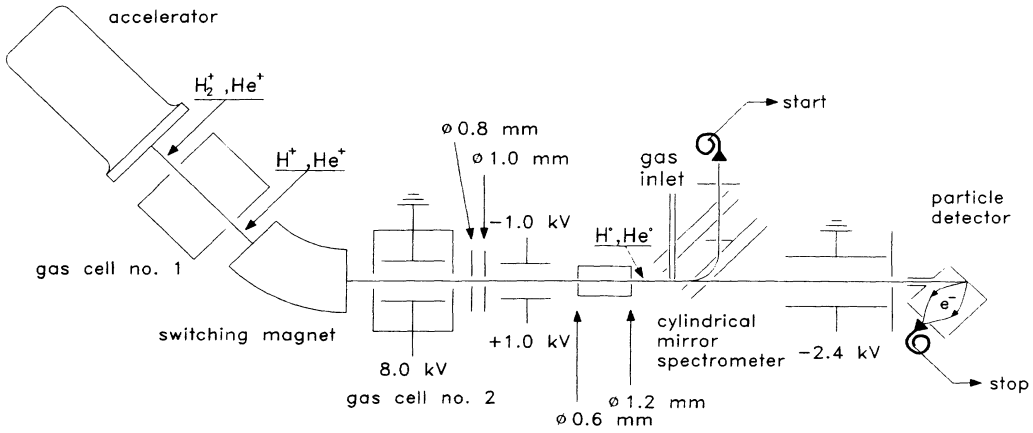

FIG. 1. Schematic view of the experimental setup.

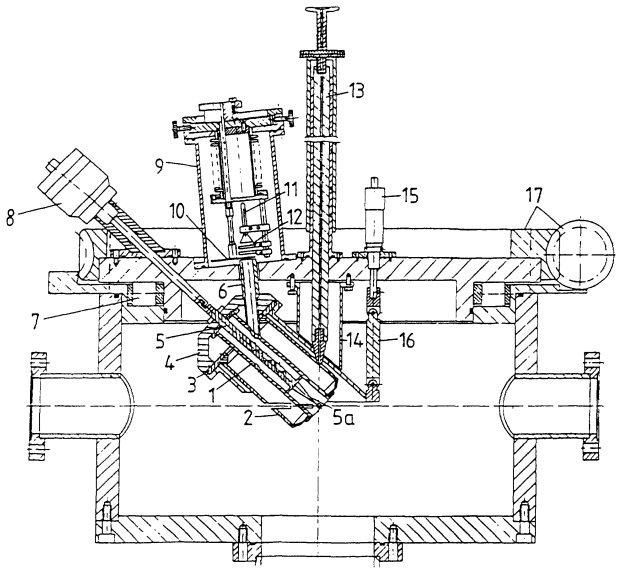

FIG. 2. Schematic view of the cylindrical-mirror electron spectrometer. The meaning of the numbers is explained in the text.

Bernardi *et al.* [16]. The spectrometer consists of two coaxial cylinders [(1) and (2)—these and the following numbers within parentheses refer to Fig. 2], which are connected by the end plates (4) with an insulating ring (3) and fixed to the top center of the chamber by means of a carrier cylinder (14). The spectrometer can be externally rotated by the φ [(15) and (16)] and Θ (17) angles, where φ is the angle around the axis perpendicular to the beam and gas-jet axes and Θ is the angle with respect to the symmetry axis of the chamber. For rotation around this axis, the whole upper part of the chamber moves on a ball track (7), driven by a worm drive. This allows us to take spectra at different angles, in the range of $0° \leq \Theta \leq 70°$, $110° \leq \Theta \leq 180°$, and $\Theta = 90°$. We assure that the spectrometer is properly aligned with respect to the beam and target axes by maximizing the electron-loss yield at 0°. Angles with respect to the beam direction can be determined and reproduced with $\pm 0.25°$ at 0°, by measuring the electron-loss intensity for positive and negative angles and assuming symmetry around zero. The inclination angle of the symmetry axis of the cylindrical-mirror spectrometer with respect to the beam direction is $\varphi_I = 42.3°$ (second-order focusing condition) [17] and could be optically controlled by the tip of a needlelike cone (5a). Interchangeable orifices allow the modification of the energy resolution [(5) and (8)], within the range $0.5\% < \Delta E/E < 7\%$, and angular acceptance (10), from 4.7×10^{-3} sr to 3.5×10^{-2} sr, of the electron spectrometer without breaking the vacuum. The angular acceptance value used in the present experiments was 2.9×10^{-2} sr ($\Theta_0 = 1.67°$). The energy resolution was chosen at moderate values ($\Delta E/E = 3.14\%$) to allow for optimized transmission properties. The vacuum in the collision chamber was kept below 10^{-6} mbar without a target; while operating the pressure-controlled gas target (13), the pressure inside the chamber could rise to approximately 10^{-5} mbar. The channeltron (11) is mounted in a differentially pumped vacuum chamber (9) with a grid system in front of it to reduce stray electrons (12). The tube (6) between the target and detector chambers acts as a field-free path region for the energy-analyzed electrons. The magnetic field of the earth inside the collision chamber between the electron source and the entrance aperture of the electron spectrometer was reduced to 3% of its original value by means of a set of electric coils.

The neutral particles were detected by two different methods depending upon whether a single-event (i.e., noncoincidence) measurement or a coincidence measurement was being performed. For the single-event measurement, the neutral projectile beam was stripped in a thin ($\rho x \approx 20$ μg/cm^2) carbon foil placed directly in front of a biased Faraday cup where the charges of the emerging H^+, respectively, He^+ or He^{2+} were collected. The stripping efficiency of such a foil is known [18] and hence a measurement of the currents determines the absolute neutral-beam intensity. For the coincidence measurement, a postcollision electric field dispersed the different charge states of the transmitted projectiles. A movable secondary-electron-emission detector [19] was adjusted to detect only one particular charge state (see Fig. 1). In the presence of the gas targets, the beam intensities ranged from $(2-5) \times 10^5$ counts per second. Without target, the charge states related to the loss process (e.g., H^+, He^+) were reduced in intensity by roughly a factor of 10. Each channel of the single-event spectra is normalized to the charge of the beam current accumulated in the Faraday Cup; the coincident electron spectra are normalized to the number of ejectiles detected in the particle detector. The relative efficiency of the secondary-electron-emission detector was checked during the measurement with the statistically distributed signals from an electric pulse generator (average 2.5 counts per second). These signals were used to gate a time window (400 nsec, that is 1.5 times the flight time of an ejectile) inside which a detected ejectile was accepted. Per channel, both the number of statistical pulses and the number of events, where an ejectile was detected within this time window, were stored in separate spectra. The first is inversely proportional to the beam current, while the latter is proportional to the beam current and to the efficiency of the particle detector. Thus the relative efficiency of the detector could be monitored by comparing these two spectra.

We used standard techniques for analyzing the electron spectra recorded noncoincidently and in coincidence with the charge-state-analyzed projectiles. Electron spectra were measured for the following cases: The sum of projectile and target ionization, as well as target single ionization and projectile single ionization, the latter of which may be accompanied by simultaneous projectile-target ionization. Standard electronics were used to process the projectile and target signals with the data being stored in list mode in a computer. Electron spectra were accumulated in 1.6-eV steps in the noncoincidence measurements and in steps of 3.2 eV for the $He^0 + Ar$ system and 6.4 eV for the remaining ones in the coincidence measurements. A typical time spectrum is shown in Fig.

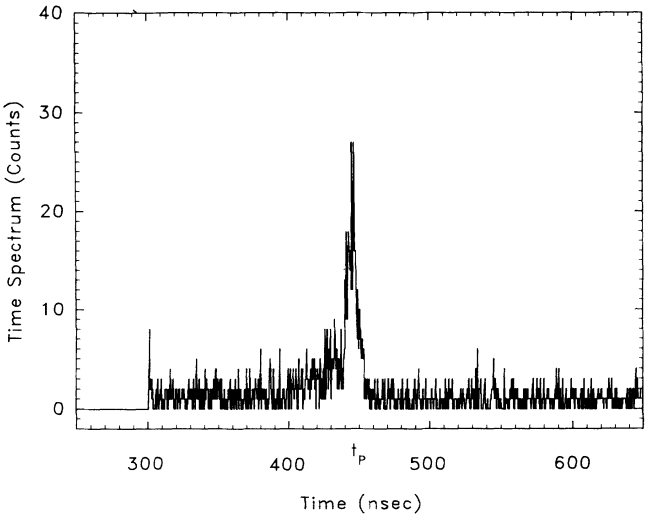

FIG. 3. Typical time spectrum. The limits of the window chosen for the time peak are 415 and 455 nsec. For the subtraction of the random background, windows at 395 and 415 nsec and 455 and 475 nsec, respectively, were chosen.

3. To analyze the true coincident events of the time spectrum at $t \approx t_p$, a window condition had been set on the time peak. The uncorrelated random background events in the time peak have been carefully subtracted by choosing window conditions in the background on both sides of the time peak and by averaging them.

Measurements for target ionization by proton impact (200 keV/u) on Ar targets at 10°, normalized to the data of Rudd, Toburen, and Stolterfoht [20], determined the target density and the detection efficiency and transmission function of the spectrometer. Using these in the neutral-beam single-event spectra, obtained under the same conditions, we were able to place the 0° noncoincident data on an absolute scale, by comparing them with the 10° ones at the binary-encounter peak, since we measured a very weak angular dependence of the transmission function. The absolute normalization of the coincidence data was performed by adding the coincident ECC and ELC spectra, corrected for the transmission function and detector efficiency of the electron spectrometer, and equating this "total" coincidence spectrum to the corresponding single-event one at the cusp maximum.

Overall absolute uncertainties are ±22% for all the single-event electron spectra and electron-loss (and double loss, in the case of He^0 projectiles) coincident spectra. For the coincident electron-capture spectra the absolute uncertainties range from 24% to 46% in the H^0 case, and from 25% to 54% for He^0. The main sources for these uncertainties are the ones quoted in the absolute data presented by Rudd, Toburen, and Stolterfoht [20], the statistical errors, and those associated with the stability of the gas target and of the accelerator beam. The statistical errors are smaller than 5% for all single-event spectra, between 3% and 8% in the electron-loss spectrum of H^0, between 11% and 30% for the ELC spectrum of He^0, ranging from 12% to 40% and from 14% to 50% in the ECC spectra of H^0 and He^0, respectively. Although the values of the absolute experimental uncertainties may appear large, one should keep in mind that the resulting absolute cross sections vary dramatically over several orders of magnitude as a function of the electron energy. Therefore the quoted uncertainties do not considerably affect the discussion of the data and the conclusions presented here. In order to assure that the coincident spectra are not superimposed on coincident electron events of the residual buffer-gas background, a coincident rest-gas spectrum was also monitored. In the case of capture, there was no substantial contribution ($<0.1\%$) due to the residual gas buffer, while in the electron-loss spectra the residual gas contribution amounted to less than 2%. Since this is mainly caused by edge and residual gas scattering, its dependence on the electron energy is very weak [3,4]. Therefore this contribution does not play any role because of the absolute normalization procedure.

III. THEORETICAL MODELS FOR ECC

Electron capture by a light, energetic projectile from a heavy target can conveniently be described within the impulse approximation [10]. The transition amplitude for the capture of a target electron with the initial state ψ_i^T into a projectile eigenstate ψ_f^P is, in the semiclassical approximation, given by (in atomic units $\hbar=m=e=1$)

$$a_{fi}=-i\int dt\int d\mathbf{k}\,\tilde{\psi}_f^{P*}(\mathbf{k}-\mathbf{v})\langle\psi_{\mathbf{k}}^T|V_P(t)|\psi_i^T\rangle \times\exp(i\mathbf{k}\cdot\mathbf{R})\exp[i(E_f-E_i-\mathbf{k}_f\cdot\mathbf{v})t]\,, \tag{3.1}$$

where $\mathbf{v}$ is the collision velocity, $\mathbf{R}=\mathbf{b}+\mathbf{v}t$ the internuclear coordinate, $E_f=k_f^2/2$ and E_i the final and initial electronic energies in the target reference frame, respectively, and $\tilde{\psi}_f^P$ the Fourier transform of ψ_f^P. The IA implies that, before being captured, the electron is excited to an intermediate target continuum state of momentum $\mathbf{k}$, $\psi_{\mathbf{k}}^T$, by means of the projectile-electron interaction V_P. For a neutral projectile, V_P is basically the static screened Coulomb potential because, for high v, polarization and exchange effects can be neglected. If use is made of the fact that the momentum-space wave function $\tilde{\psi}_f^P(\mathbf{k}-\mathbf{v})$ is strongly peaked at $\mathbf{k}=\mathbf{k}_f=\boldsymbol{\kappa}_f+\mathbf{v}$ (where $\boldsymbol{\kappa}_f$ is the electronic momentum in the projectile frame), one achieves a considerable simplification by setting $\mathbf{k}=\mathbf{k}_f$ throughout in the remainder of the integrand in Eq. (3.1). In this so-called "full-peaking" approximation the differential cross section for electron capture factors into the cross section for target ionization to a state $\psi_{\mathbf{k}_f}^T$ times the normalization constant of the projectile eigenstate, $\psi_f^P(\mathbf{r}=\mathbf{0})$:

$$\frac{d^2\sigma}{dE_f d\Omega_f}=(2\pi)^3|\psi_f^P(\mathbf{r}=\mathbf{0})|^2\sum_i\frac{d^2\sigma_i^I}{dE_f d\Omega_f}\,,$$
$$\frac{d^2\sigma_i^I}{dE_f d\Omega_f}=\frac{2\pi}{v}N_i k_f\int d\mathbf{q}\,\delta(E_f-E_i-\mathbf{q}\cdot\mathbf{v}) \times|\tilde{V}_P(\mathbf{q})\langle\psi_{\mathbf{k}_f}^T|\exp(i\mathbf{q}\cdot\mathbf{r})|\psi_i^T\rangle|^2\,, \tag{3.2}$$

where the sum runs over the subshells i of the target with occupation numbers N_i, and $\tilde{V}_P(\mathbf{q})$ is the Fourier transform of $V_P(t)$. A necessary condition for the validity of the peaked IA is $Z_{P,\text{eff}} \ll Z_T/n_i$ and $v \gg Z_T/n_i$, where $Z_{P,\text{eff}}$ is the effective projectile charge, Z_T is the nuclear target charge, and n_i the main quantum number of the initial state. Equation (3.2) allows for a separation of the properties of the projectile-scattering state, which determines the shape of the forward peak, from the target-excitation process, which provides the background in the peak region. We shall concentrate on the former and distinguish three cases.

(a) Bare projectiles (H^+, He^{2+}). In this case, ψ_f^P is a Coulomb wave which diverges near threshold ($\kappa_f = 0$) according to

$$(2\pi)^3 |\psi_f^P(\mathbf{r}=\mathbf{0})|^2 \approx \frac{2\pi Z_p}{\kappa_f}, \quad \kappa_f \to 0 \tag{3.3}$$

and hence causes a cusplike peak with a width proportional to the detector resolution Θ_O.

(b) Partially stripped or neutral projectiles in their ground state [$H^0(1s)$, $He^+(1s)$, $He^0(1s^2)$]. Assuming that the projectile electrons are not affected during the collision, the capture cross section is given by Eq. (3.2), with the projectile-scattering state ψ_f^P calculated from a Schrödinger-type equation which for hydrogen- or heliumlike systems reads [21]

$$[-\tfrac{1}{2}\Delta + V_P(\mathbf{r})]\psi_f^P(\mathbf{r}) + (-1)^J \left[\left\langle \varphi_i(\mathbf{r}') \left| \frac{1}{|\mathbf{r}-\mathbf{r}'|} \right| \psi_f^P(\mathbf{r}') \right\rangle - (E\kappa_f - \varepsilon_i)\langle \varphi_i(\mathbf{r}')|\psi_f^P(\mathbf{r}')\rangle \right] \varphi_i(\mathbf{r}) = E\kappa_f \psi_f^P(\mathbf{r}') , \tag{3.4}$$

where the term in large parentheses accounts for exchange and orthogonality to the bound state $\varphi_i(\mathbf{r})$ with energy ε_i. The total spin is denoted by J, and $E_f = \kappa_f^2/2$. For the normalization constant of $\psi_f^P(\mathbf{r})$, only the zeroth partial wave of (3.4) is required. The result is a cusplike forward peak for partly stripped projectiles, and a broad peak for neutral projectiles [11]. The existence of a peak for neutral atoms (and the enhancement of the cusp for ions beyond the value expected from the ionic charge) is caused by the attractive polarization field which, for low momenta κ_f, has to be included in V_P.

(c) Neutral projectiles in an excited state [$H^0(2s)$, $He^0(1s2s)$]. As has been pointed out by Garibotti and Barrachina [22], a transiently occurring s-wave virtual state of the negative ion (consisting of the excited neutral projectile and the electron to be captured) may considerably affect the peak shape. A near-threshold shape resonance of the negative ion will have a similar effect. From general scattering theory [23] it can be inferred that the normalization constant of ψ_f^P is given by the inverse of the Jost function which becomes zero at a resonance. For κ_f in the vicinity of the resonance, a linear expansion of the Jost function is possible, so that

$$(2\pi)^{3/2}\psi_f^P(\mathbf{r}=\mathbf{0}) = \frac{1}{A(\kappa_f - p_R + ip_I)} , \tag{3.5}$$

where the resonance is assumed to be at the complex momentum $\kappa_R = p_R - ip_I$, and A is a constant. In the case of a shape resonance, the values of p_R and p_I are determined from the energy E_R and width Γ of the resonance, by means of $E_R - i\Gamma/2 = \kappa_R^2/2$. For H^- there is a p-wave resonance at $E_R = 0.018$ eV with $\Gamma = 0.021$ eV [24], which couples strongly into the s-wave channel through Stark mixing and which has a sufficiently small energy to fall into the cusp region. The constant A can tentatively be related to the current which results from the decay of the resonance [25] such that one obtains a Breit-Wigner-type expression

$$(2\pi)^3 |\psi_f^P(\mathbf{r}=\mathbf{0})|^2 \approx \frac{2p_R p_I}{(\kappa_f - p_R)^2 + p_I^2} . \tag{3.6}$$

It should be noted that this expression is only valid for $\kappa_f \to p_R$ with $p_R \geq p_I$. Off resonance, e.g., in the outer wings of the ECC peak, a background contribution [which is suppressed in (3.6)], which may be obtained from an equation similar to (3.4), with the ground-state functions and potentials replaced by the corresponding quantities for an excited state, will gain importance.

In the case of a virtual state, one has, according to definition, $p_R = 0$. For He^-, there is a virtual state slightly below the 2^1S threshold with $p_I = 3.0215 \times 10^{-3}$ a.u. [26]. Equation (3.6) should then be replaced by

$$(2\pi)^3 |\psi_f^P(\mathbf{r}=\mathbf{0})|^2 \approx \frac{2p_I^2}{\kappa_f^2 + p_I^2}, \quad \kappa_f \to 0 . \tag{3.7}$$

With p_I very small, Eqs. (3.6) and (3.7) lead to a cusplike forward peak which is narrower than the one for a Coulombic field, since $|\psi_f^P(\mathbf{r}=\mathbf{0})|^2$ behaves approximately like κ_f^{-2}. The virtual state for He^- has been used by Barrachina [12] to interpret the experimental results of Sarkadi *et al.* [7]. However, the comparison with experiment was not made on an absolute scale.

When the beam consists exclusively of ground-state atoms, the occurrence of a virtual state or a shape resonance is only possible if the projectiles get excited during the collision prior to capture. Using again the IA, the transition amplitude for this process is given by

$$a_{fi} = -i \int dt \int d\mathbf{k}\, \tilde{\psi}_f^{P*}(\mathbf{k}-\mathbf{v}) \langle \Phi_f^P \psi_{\mathbf{k}}^T | [V_{ee}(t) + V_P(t) G_{0i} V_T(t)] | \Phi_i^P \psi_i^T \rangle \exp(i\mathbf{k}\cdot\mathbf{R}) \exp[i(E_f - E_i - \mathbf{k}_f\cdot\mathbf{v} + \Delta E^P)t] , \tag{3.8}$$

where Φ_i^P, Φ_f^P ($f \neq i$) are the wave functions of the initial and final projectile electronic states, respectively, ΔE^P is their energy difference, and $G_{0i}=(i\partial_t - H_{0i}+i\varepsilon)^{-1}$, where H_{0i} is the unperturbed Hamiltonian of the initial state, describing the separated projectile and target atoms. The first-order term, where the transition is mediated by the electron-electron coupling V_{ee}, accounts for the simultaneous projectile excitation and electron capture. Only this term has been considered by Barrachina [12]. From electron-loss calculations we know, however, that second-order couplings via the nuclear potentials are dominant for high-momentum transfers. Hence we have included in (3.8) a term which describes the projectile excitation by means of the static screened target potential V_T, followed by electron capture induced by V_P. In V_P, screening is due to the *excited* electron. Another second-order term which describes electron capture prior to projectile excitation has been omitted as not being relevant. Concentrating only on the second term in Eq. (3.8) and applying the full-peaking approximation, the cross section is given by

$$\frac{d^2\sigma}{dE_f d\Omega_f} \approx (2\pi)^3 |\psi_f^P(\mathbf{r}=0)|^2 \sum_i \frac{k_f N_i}{(2\pi)^2 v} \int d\mathbf{q}\, \delta(E_f - E_i - \mathbf{k}_f\cdot\mathbf{v} + \Delta E^P - \mathbf{q}\cdot\mathbf{v}) \times \left| \int d\mathbf{p}\, \tilde{V}_T(\mathbf{p}) \frac{1}{\Delta E^P + \mathbf{p}\cdot\mathbf{v} - i\varepsilon} \langle \Phi_f^P | \exp(i\mathbf{p}\cdot\mathbf{r}) | \Phi_i^P \rangle \tilde{V}_P(\mathbf{q}+\mathbf{k}_f+\mathbf{p}) \times \langle \psi_{\mathbf{k}_f}^T | \exp[i(\mathbf{q}+\mathbf{k}_f+\mathbf{p})\cdot\mathbf{r}] | \psi_i^T \rangle \right|^2 . \quad (3.9)$$

A second peaking approximation ($p_\perp = 0$) is made in V_P and the target ionization matrix element in the further calculation. For the target and projectile states, Slater-screened hydrogenic functions and experimental binding energies have been used to account for the passive electrons.

IV. RESULTS AND DISCUSSION

In Fig. 4(a) we present the absolute DDCS obtained from the single-event and coincident electron spectra at 0° for H^0 (200-keV) projectiles impinging upon Ar targets, together with the absolute DDCS from the single-event spectrum for incident protons with the same energy and electron-emission angle. The coincidence spectra represent the capture (coincidence with H^0 ejectiles) and loss (coincidence with H^+-emergent-charge-state) processes. It can be seen from this figure that the loss process accounts for almost all electron emission in the forward direction, capture being less than 1% in the energy region around the cusp. It can also be seen that the ECC data for H^0 are approximately one order of magnitude smaller than those for protons, demonstrating the screening effect by the passive projectile electron. For the sake of comparison, we present in Fig. 4(b) the same spectra as in the previous figure, all normalized to 1 at the cusp maximum (i.e., electron energy of 112 eV). As expected, the ELC cusp from H^0 projectiles is approximately symmetric while the ECC cusp from proton impact has a larger width and is skewed to the low-energy side. It is also clearly seen that the ECC cusp from H^0 is considerably narrower than the ELC cusp.

The lower part of Fig. 5 shows the H^0+Ar ECC data in comparison with theory. Only capture from the Ar M

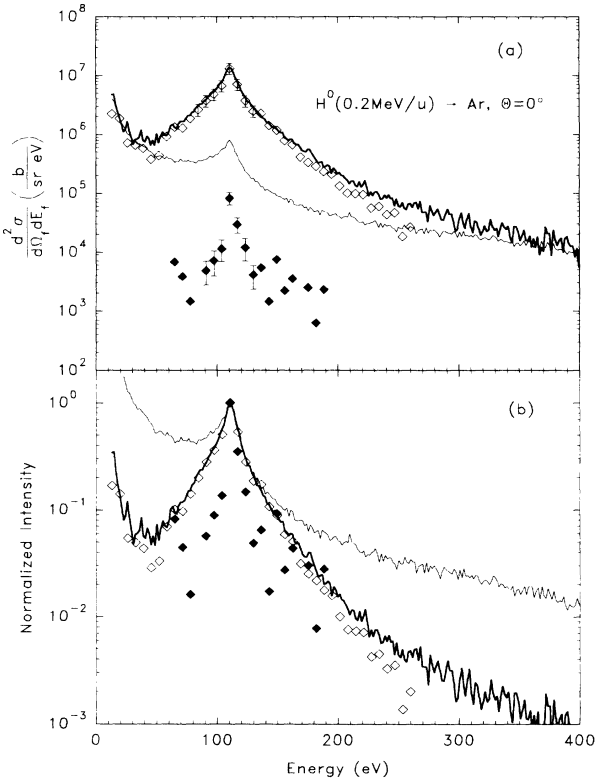

FIG. 4. (a) Absolute DDCS at 0° for 200-keV H^0 and H^+ impact on Ar. —— (heavy solid line), single-event H^0 data; —— (light solid line), single-event H^+ data; ◆, coincident ECC H^0 data; ◇, coincident ELC H^0 data; (b) same spectra as above, but, for ease of comparison, normalized to 1 at the cusp maximum.

shell has been considered, the contributions from the inner shells being negligibly small. It is seen that ECC into ground-state atoms (assuming a singlet state of H^-) leads to a rather broad forward peak. If the experimental data were tentatively decomposed into a narrow peak and a background which is much less energy dependent, the shape of the background could reasonably well be described with that theory. The intensity is, however, considerably above the data (in the figure, the ground-state ECC curve has been scaled down by a factor of 5). This may be ascribed to the deficiency of the full-peaking approximation for the rather low impact velocity ($vn_M/Z_{T,\text{eff}} \sim 1$, $Z_{T,\text{eff}}$ being equal to 6.75 for the Ar M shell). For the case of proton impact, experiment is similarly overestimated by the peaked IA (by a factor of 2.8 in the peak maximum).

The results for ECC from (metastable) excited atoms show a sharp peak due to the presence of the shape resonance. Although averaged over the experimental angular and energy resolutions, the calculated peak width is a factor of 2 smaller than the experimental value. The depicted curve is unscaled and assumes that all projectiles are in metastable states. This assumption is, however, inconsistent with the experimental conditions. Since practically all H^0 beam particles are in their ground state, the process of projectile excitation prior to ECC has also been considered. The shape of the peak is very much the same as in the case of metastable beam particles, but the intensity falls below the latter by a factor of 0.023 and hence is much too small to play any role. An excitation probability of H^0 in the percent region has also been found from experimental results [24]. Figure 6(a) shows the absolute experimental DDCS for He^0 projectiles impinging upon Ar. The gross features of the spectra are similar to those for H^0 impact with the exception that the coincident ECC data only fall about a factor of 20 below the single-ELC data and the full width at half maximum (FWHM) of the coincident ECC peak is approximately a factor of 3 larger than the one measured for H^0. Double ELC has also been measured. Its intensity is, however, much smaller than for single-electron loss. The peak width for double ELC is larger than for single ELC, as is obvious from Fig. 6(b), where all data are normalized to unity in the maximum, and there is a considerable skewness to the low-energy side, pointing to higher-order effects (beyond first-order Born) at such a low collision velocity. In-

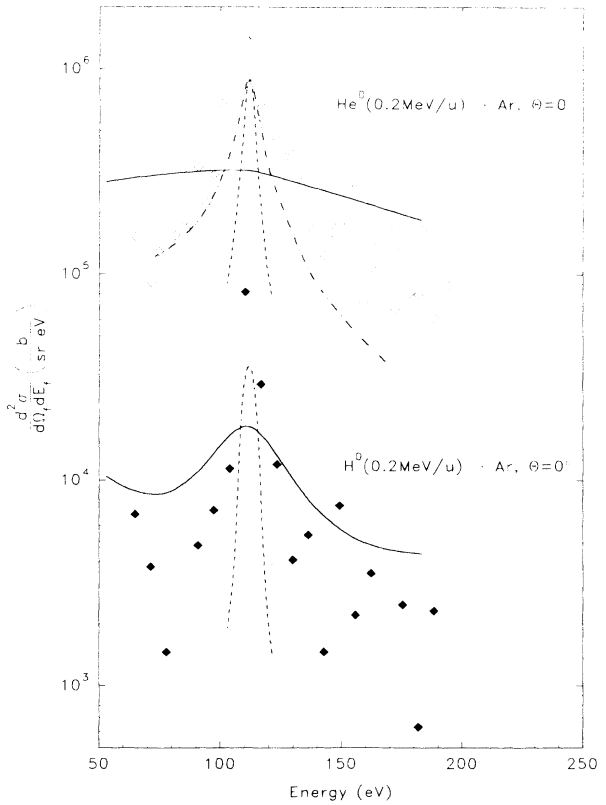

FIG. 5. Absolute DDCS for ECC in collisions of 200 keV/u He^0 (upper part) and H^0 (lower part) with Ar as a function of electron energy. Experiment: DDCS in coincidence with transmitted He^0 (◇) and H^0 projectiles (◆), respectively. Theory (peaked IA): ——, ECC by ground-state projectiles (for H^0 projectiles the cross section is divided by 5); — — —, ECC by projectiles with one electron in the $2s$ state (for He^0 projectiles the cross section is multiplied by 2×10^3); –·–·–, ECC by He^{2+} (scaled down by a factor of 20 to coincide with the dashed line in the maximum). The peak position ($v^2/2$) is at 112 eV.

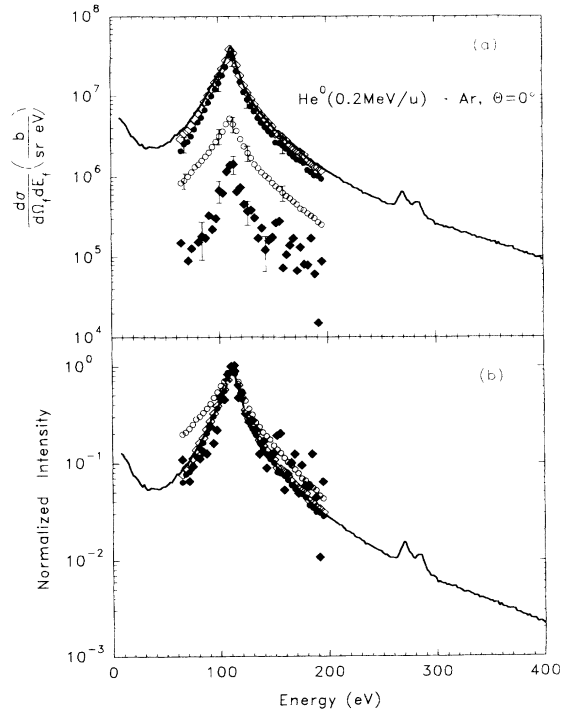

FIG. 6. (a) Absolute DDCS at 0° for 200-keV/u He^0 impact on Ar. ——, single-event He^0 data; ⧫, coincident ECC He^0 data; ⧫, coincident single-ELC He^0 data; ⧫, coincident double-ELC He^0 data; ◇, coincident single-plus double-ELC data; (b) same spectra as above, but, for ease of comparison, normalized to 1 at the cusp maximum.

terestingly, the width of the He^0 ECC peak is nearly as large as that of the single, ELC, whereas Sarkadi *et al.* and Berényi *et al.* have found a much narrower peak [7,8]. Taking into account the scaling with $v\Theta_O$ [2], the ratios of the FWHM between the present data and the ones of those authors are approximately 3 for H^0 and 8.5 for He^0 projectiles. One can also observe in this figure the kinematically shifted autoionization peaks of the He^0 projectile, located approximately at 270 and 285 eV.

The comparison of the experimental ECC peak for the He^0+Ar system with the theoretical predictions is shown in the upper part of Fig. 5. The calculated spectrum for ECC by ground-state projectiles has only a very weak maximum in contrast to the H^0 case due to the smaller polarization potential and the different spatial symmetry of the negative ion state. Assuming a 30% contribution of metastable He^0 atoms in the beam, the ground-state ECC (shown in the figure for a pure ground-state beam) should be scaled down by a factor of 0.7 and hence would give a reasonable account for the experimental background. On the other hand, for the case of metastable excited projectiles with consideration of the virtual resonant state, the resulting cusp is not only far too narrow as compared with experiment, but also, due to the averaging over the detector resolution, this extremely sharp resonance decreases considerably in intensity (the curve shown in the figure, assuming 100% metastable states in the beam, is scaled up by a factor 2×10^3). Assuming projectile excitation during the encounter with the target, the resulting cusp intensity is further reduced (as compared to the case of an already excited beam) by a factor of 0.066. Tentatively, we have included in the figure the cusp shape of ECC by He^{2+}; we find that this shape would account much better for the experimental data. However, there is no experimental evidence for the existence of charged He ions in the beam.

The exploratory data obtained with the He targets, although with many fewer events, present the same general features discussed above, such as, for example, similar ratios between ELC and ECC at the cusp maximum [27].

V. CONCLUSION

We have measured cusp-shaped electron spectra in collisions of H^0, H^+, and He^0 on helium and argon. By detecting the charge states of the transmitted projectiles in coincidence with the electrons we were able to distinguish between electron capture and single- or double-electron loss to the continuum of the projectile. In the case of ECC by neutral projectiles, we have confirmed the existence of a cusplike peak, which had previously been discovered in slower He^0+Ar collisions [7]. Absolute measurements of the doubly differential electron-emission cross section allowed a detailed comparison with the various capture theories. Interpreting the coincident ECC spectra as being composed of a sharp peak superimposed on a background with a broad peak, we tentatively ascribe the background to ECC by ground-state neutral projectiles. There is, however, no convincing evidence that the sharp peak is caused by a virtual state or a shape resonance of the transiently formed excited negative ion. Taking into consideration that the fraction of metastable states in the H^0 beam is below 1%, the intensity of the calculated cusp is two orders of magnitude too small. For He^0, not only is the theoretical intensity far too low, even when considering a 30% fraction of metastable atoms in the incoming beam, but also the cusp width is much smaller than the measured one. A conclusive interpretation of this discrepancy between theory and experiment requires not only further systematic experiments involving other collision systems and velocities, but also the development of new theoretical models.

ACKNOWLEDGMENTS

This work has been funded by the German Federal Minister for Research and Technology (BMFT) under Contract Number 06 OF110 Ti476 and by the GSI Darmstadt. One of the authors (G.M.S.) acknowledges the hospitality in the IKF and partial support from the Coordenaçao de Aperfeiçoamento de Pessoal de Nivel Superior (CAPES), Brasil.

*On leave of absence from Departamento de Fisica, Pontificia Universidade Católica, Caixa Postal 38071, Rio de Janeiro 22453, Brazil.

†Permanent address: Sektion Physik, Universität München, Am Coulombwall 1, D-8046 Garching, Germany.

‡Present address: Lahmeyer International GmbH, Frankfurt/Main, Germany.

[1] G. B. Crooks and M. E. Rudd, Phys. Rev. Lett. **25**, 1599 (1970).

[2] *Proceedings of a Symposium on the Forward Electron Ejection in Ion-Atom Collisions,* edited by K. O. Groeneveld, W. Meckbach, and I. A. Sellin, Lecture Notes in Physics Vol. 213 (Springer-Verlag, Heidelberg, 1984).

[3] O. Heil, R. D. DuBois, R. Maier, M. Kuzel, and K. O. Groeneveld, Z. Phys. D **21**, 235 (1991).

[4] O. Heil, R. D. DuBois, R. Maier, M. Kuzel, and K. O. Groeneveld, Phys. Rev. A **45**, 2850 (1992).

[5] M. Breinig, S. B. Elston, S. Huldt, L. Liljeby, C. R. Vane, S. D. Berry, G. A. Glass, M. Schauer, I. A. Sellin, G. D. Alton, S. Datz, S. Overbury, R. Laubert, and M. Suter, Phys. Rev. A **25**, 3015 (1982).

[6] J. Macek, Phys. Rev. A **1**, 235 (1970).

[7] L. Sarkadi, J. Palinkás, A. Kövér, D. Berényi, and T. Vajnai, Phys. Rev. Lett. **62**, 527 (1989).

[8] D. Berényi, L. Sarkadi, L. Gulyás, A. Kövér, Gy. Szabó, and J. Pálinkás (unpublished).

[9] K. Kroneberger, G. M. Sigaud, H. Rothard, O. Heil, A. Albert, R. Maier, D. Schlösser, M. Schosnig, H. Trabold, and K. O. Groeneveld, Nucl. Instrum. Methods B (to be published) and references therein.

[10] J. S. Briggs, J. Phys. B **10**, 3075 (1977).

[11] D. H. Jakubassa-Amundsen, J. Phys. B **22**, 3989 (1989).

[12] R. O. Barrachina, J. Phys. B **23**, 2321 (1990).

[13] L. Szótér, Phys. Rev. Lett. **64**, 2835 (1990).
[14] E. Horsdal-Pedersen, J. Heinemeier, L. Larsen, and J. V. Mikkelsen, J. Phys. B **13**, 1167 (1980).
[15] I. A. Sellin, Phys. Rev. A **136**, 1425 (1964).
[16] G. Bernardi, S. Suárez, P. Focke, and W. Meckbach, Nucl. Instrum. Methods B **33**, 321 (1988).
[17] J. S. Risley, Rev. Sci. Instrum. **43**, 95 (1972).
[18] H. D. Betz, in *Applied Atomic Collision Physics*, edited by S. Datz (Academic, London, 1983), Vol. 4, p. 1.
[19] K. Rinn, A. Müller, H. Eichenauer, and E. Salzborn, Rev. Sci. Instrum. **53**, 829 (1982).
[20] M. E. Rudd, L. H. Toburen, and N. Stolterfoht, At. Data Nucl. Data Tables **23**, 405 (1979).
[21] H. Nakanishi and D. M. Schrader, Phys. Rev. A **34**, 1810 (1986).
[22] C. R. Garibotti and R. O. Barrachina, Phys. Rev. A **28**, 2792 (1983).
[23] J. R. Taylor, *Scattering Theory* (Wiley, New York, 1972), p. 205.
[24] F. Penent, J. P. Grouard, J. L. Montmagnon, and R. I. Hall, J. Phys. B **24**, 173 (1991).
[25] L. D. Landau and E. M. Lifschitz, *Quantum Mechanics* (Pergamon, London, 1959), Vol. III, Secs. 50, 131, and 132.
[26] R. K. Nesbet, J. Phys. B **13**, L193 (1980).
[27] H. Trabold, Diploma thesis, Institut für Kernphysik, J. W. Goethe Universität, Frankfurt am Main, 1991.